Room-temperature defect-engineered spin filter based on a non-magnetic semiconductor.

Xingjun Wang, I A Buyanova, F Zhao, D Lagarde, A Balocchi, X Marie, C W Tu, J C Harmand and Weimin Chen

Original Publication:

Xingjun Wang, I A Buyanova, F Zhao, D Lagarde, A Balocchi, X Marie, C W Tu, J C Harmand and Weimin Chen, Room-temperature defect-engineered spin filter based on a non-magnetic semiconductor., 2009, Nature Materials, (8), 3, 198-202.
http://dx.doi.org/10.1038/nmat2385

Room temperature defect-engineered spin filter based on a non-magnetic semiconductor

X.J. Wang[1], I.A. Buyanova[1], F. Zhao[2], D. Lagarde[2], A. Balocchi[2], X. Marie[2], C.W. Tu[3], J.C. Harmand[4] and W.M. Chen[1*]

[1]Department of Physics, Chemistry and Biology, Linköping University, 58183 Linköping, Sweden

[2]Université de Toulouse, LPCNO: INSA, UPS, CNRS, 135 avenue de Rangueil, 31077 Toulouse cedex, France

[3]Department of Electrical and Computer Engineering, University of California, La Jolla, CA92093, USA

[4]LPN, route de Noazay, 91460 Marcoussis, France

* e-mail: wmc@ifm.liu.se

Generating, manipulating and detecting electron spin polarization and coherence at room temperature (RT) is at the heart of future spintronics and spin-based quantum information technology[1-4]. Spin filtering, which is a key issue for spintronic applications, has been demonstrated by employing ferromagnetic metals[5-8], diluted magnetic semiconductors[9,10], quantum point contacts[11], quantum dots[12], carbon-nanotubes[13] and multiferroics[14], etc. This filtering effect was so far restricted to a limited efficiency and primarily at low temperatures or under a magnetic field. Here, we provide direct and unambiguous experimental proof that an electron spin-polarized defect, such as a Ga_i self-interstitial in dilute nitride GaNAs, can effectively deplete conduction electrons with an opposite spin orientation and can thus turn the non-magnetic semiconductor into an efficient spin filter operating at RT and zero magnetic field. This work shows the potential of such defect-engineered, switchable spin filters as an attractive alternative to generate, amplify and detect electron spin polarization at RT without a magnetic material or external magnetic fields.

In Fig.1a we illustrate the physical principle of the approach. If an electron localized at a defect is spin polarized, the defect will only capture a conduction electron with an opposite spin due to the Pauli exclusion principle and can subsequently annihilate it with a hole. If the corresponding process is efficient, spin-polarized defects will effectively deplete the conduction electrons with the opposite spin and will leave behind only those with the same spin as the defect electrons. This process will turn a pool of spin-unpolarized electrons entering the material into spin-polarized ones when they exit, making the material a spin filter. The incoming electrons to be spin filtered as well as the spin polarization of the electrons at the defects can be provided either by electrical injection or by optical excitation, making this versatile spin filter relevant to a variety of applications in future spin electronics or spin photonics.

For a proof of concept purpose, we employed optical excitation and detection as illustrated in Fig.1b-c. We show below that Ga_i self-interstitials in GaNAs are identified as suitable defects for efficient spin filtering. This is because each Ga_i is occupied by a single electron in the doubly positively charged state Ga_i^{2+}. When this electron is spin polarized, the defect can efficiently capture a conduction electron with an opposite spin and subsequently rapidly annihilate with a free hole. The complete carrier recombination path is identified as: $Ga_i^{2+} \xrightarrow{photo-excitation} Ga_i^{2+}+e+h \xrightarrow{e\ \ capture} Ga_i^{1+}+h \xrightarrow{h\ \ capture} Ga_i^{2+}$. Spin polarization of the electrons at Ga_i^{2+} was provided by optical orientation[15] using circularly polarized light ($\sigma^{\pm}$) via spin-dependent recombination (SDR)[16-21], as described in the "Methods" section . The spin-filtering effect induced by the spin-polarized defects drives the spins of the conduction and localized electrons at Ga_i^{2+} towards complete alignment when no further electron capture and recombination can occur via the defects as shown in Fig.1b. Consequently, a high degree of conduction electron spin polarization P_e can be achieved. P_e is

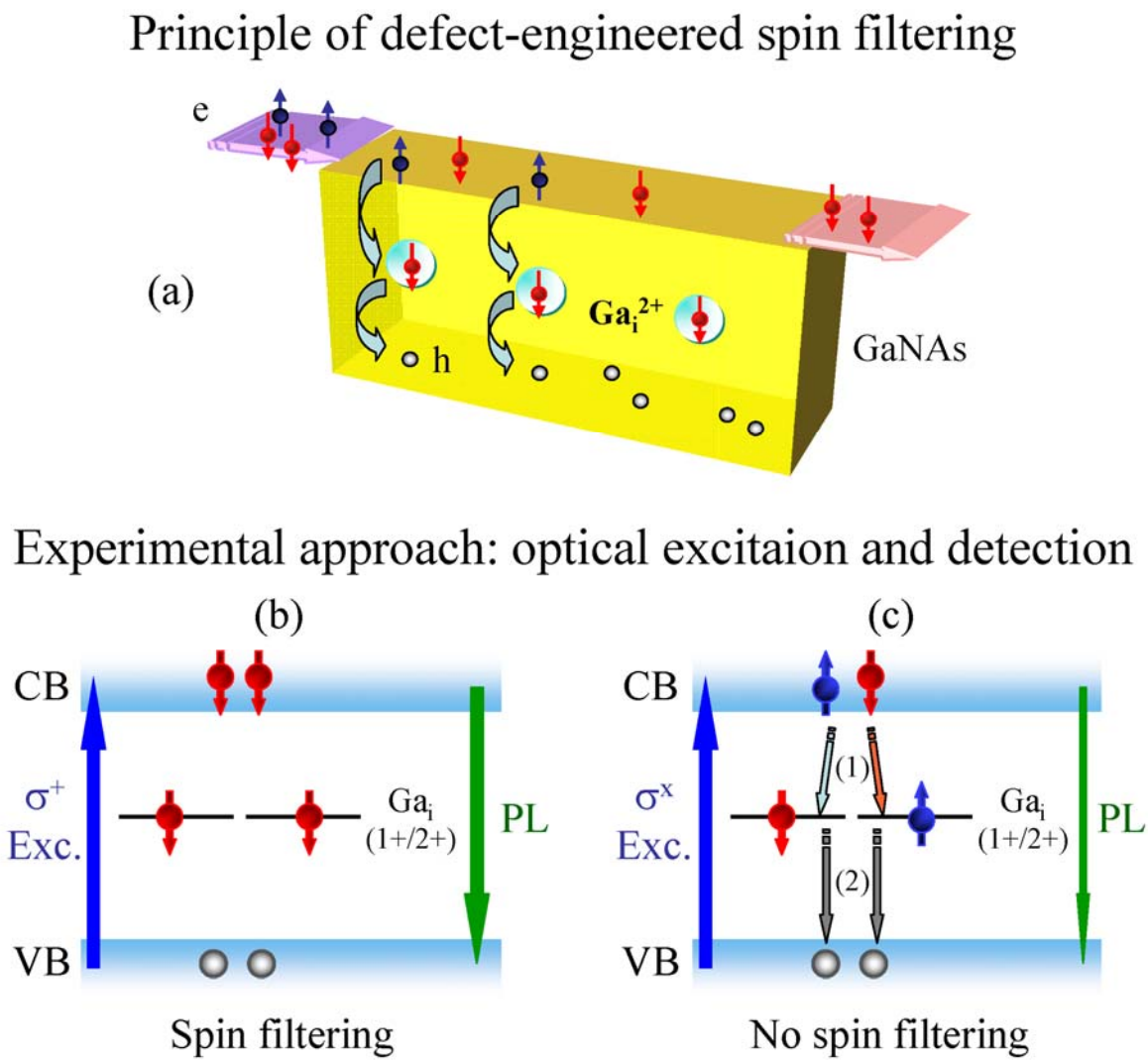

Figure 1: Principle of defect-engineered spin filtering and the experimental approach at RT and B=0. *(a) A schematic illustration of the spin filtering effect of conduction electrons via spin-polarized defects in a non-magnetic semiconductor, e.g., Ga_i self-interstitials in GaNAs. (b) In our approach, spin polarization of the first electrons at the defects is achieved by circularly polarized photo-excitation (σ^+ as an example), leading to the spin filtering effect and spin blockade of carrier recombination via the defects when both conduction and defect electrons are completely polarized to the same spin orientation. Consequently, higher free carrier concentrations and thus stronger intensity of the associated band-to-band (BB) PL transition are expected in case (b) as compared with case (c). (c) As a reference in our approach, linearly polarized photo-excitation (σ^x) corresponds to the case when no spin polarization of the first electrons at the defects can be created and thus no spin filtering effect is expected. CB and VB denote the conduction band and valence band, respectively. The charge transition (1+/2+) of the spin-filtering Ga_i defects is also indicated, corresponding to a transition between Ga_i^{1+} and Ga_i^{2+} that have two and one bound electrons, respectively. The numbers in the parentheses associated with the electron capture and annihilation via the defects shown in (c) indicate the sequence of events. The thickness of the PL arrows symbolizes the relative intensity of the BB transition.*

defined as $P_e = \frac{n_+ - n_-}{n_+ + n_-}$, where n_+(n_-) denotes the spin-up (spin-down) conduction electron concentration. For comparison, linearly polarized optical excitation (σ^x) was also employed.

Such excitation equally generates electrons of both spins, and will thus lead to zero electron spin polarization of the defects at zero magnetic field (B=0). Now, the defect can capture conduction electrons of both spins with an equal probability (Fig.1c), i.e., spin filtering ceases to function. This leads to zero P_e and shorter lifetimes for the photo-generated carriers as compared to that under $\sigma^{\pm}$ excitation, which can be monitored by photoluminescence (PL) of the band-to-band (BB) transition.

In Fig.2a we show the BB PL spectrum from GaNAs obtained at RT and B=0. It consists of the strongly overlapping electron-heavy hole (e-hh) and electron-light hole (e-lh) transitions, which split under the tensile strain leaving the e-hh emission at the shorter wavelength[22]. The PL polarization of these transitions, defined by $\frac{I(\sigma^+)-I(\sigma^-)}{I(\sigma^+)+I(\sigma^-)}$ where $I(\sigma^+)$ and $I(\sigma^-)$ denote PL intensities with the corresponding polarizations, directly reflects P_e. (Due to strong spectral overlap with the more intense e-hh emission with opposite PL polarization, the PL polarization of the e-lh emission is severely undermined in the measured spectra.) $P_e=-\frac{I(\sigma^+)-I(\sigma^-)}{I(\sigma^+)+I(\sigma^-)}$ when only the e-hh transition is considered, which is used below to obtain P_e. It should be pointed out that the actual P_e values should be higher than that deduced in this way when hh-lh mixing and spectral overlap are taken into account. Under σ^x excitation, zero P_e was observed as expected. Under $\sigma^{\pm}$ excitation, on the other hand, a sizable P_e can be detected. Its sign can be changed following a change in the helicity of the excitation light. P_e was found to critically depend on N composition and growth conditions, which determine the concentration of Ga_i. The observed values (~32%) are much higher than that observed in N-free GaAs (< 6%), being a direct consequence of the strong spin filtering effect due to Ga_i preferably introduced in GaNAs. The observed strong P_e is accompanied by a higher PL intensity under $\sigma^{\pm}$ excitation than that under σ^x excitation (Fig.2b-c). This arises

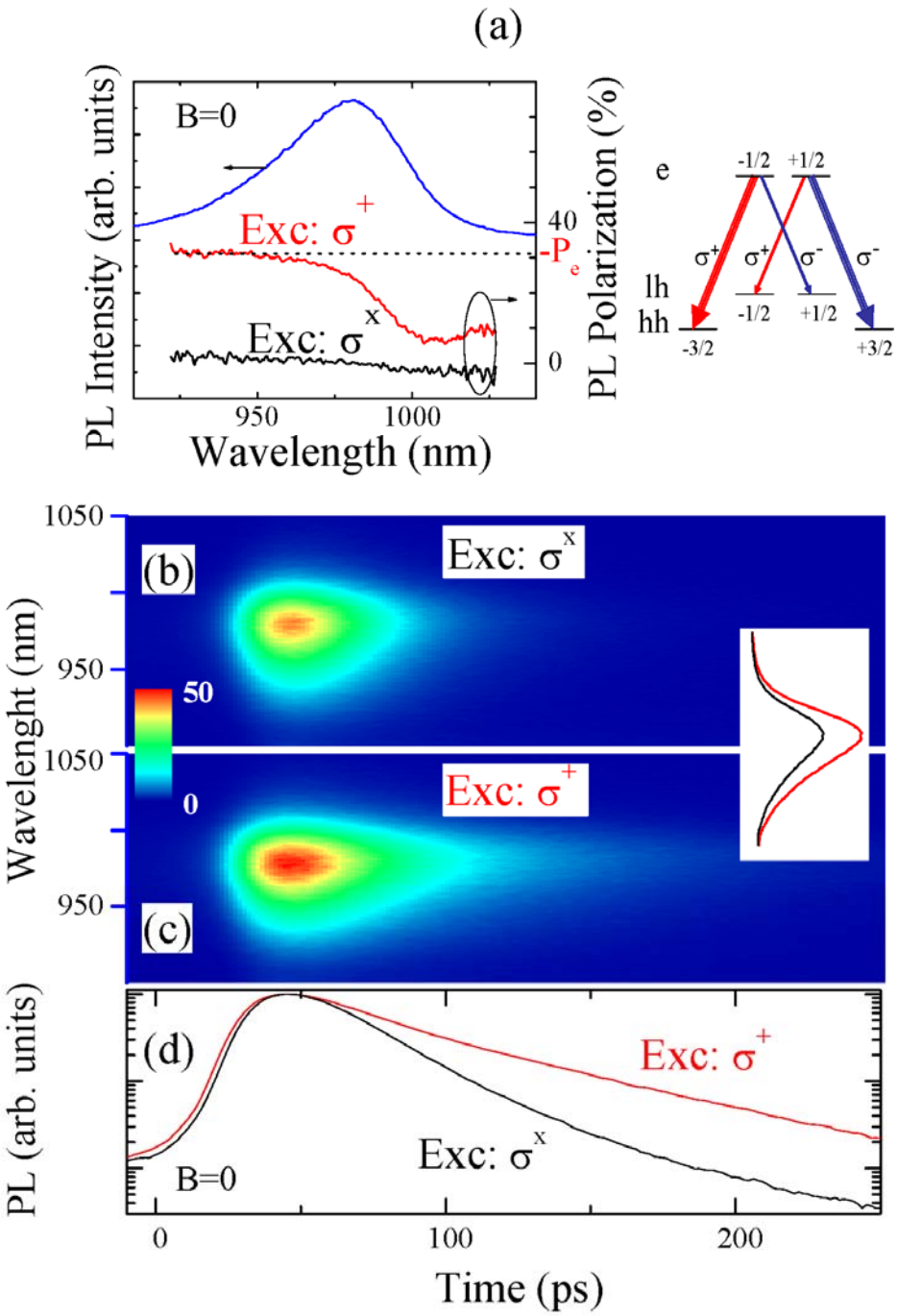

Figure 2: PL intensity and polarization (i.e., corresponding to the conduction electron spin polarization P_e) with or without the spin filtering effect. *(a) A typical BB PL spectrum under σ^x excitation, and PL polarization obtained under σ^x and σ^+ excitation. A schematic picture of the CB and VB states and the associated e-hh and e-lh transitions is also shown. The notations ±1/2 and ±3/2 refer to $\left|m_s^c\right\rangle$ and $\left|m_J^v\right\rangle$ of the conduction and valence band electrons. (b) and (c) Temporal evolution of the BB PL spectra (by detecting the total PL intensity) after σ^x and σ^+ polarized pulsed laser excitation, respectively. Time-integrated PL spectra, under σ^x (black curve) and σ^+ (red curve) excitation, are shown in the inset. (d) Decay curves of the total intensity of the BB PL under σ^x and σ^+ excitation, normalized to their peak intensity for easy comparison. All results were obtained from the as-grown $GaN_{0.0076}As_{0.9924}$ epilayer grown at 420 °C. The wavelength of the excitation photons is 840 nm. All results were obtained at RT and B=0.*

from spin blockade of the Ga_i-mediated carrier recombination under $\sigma^{\pm}$ excitation, consistent with the slower PL decay shown in Fig.2b-d.

To obtain quantitative information on the concentration of spin-filtering defects and their effect on P_e, we carried out a detailed study of P_e dependence on excitation light intensity (i.e. on the number of photo-generated free carriers). Representative results obtained at RT and B=0 are shown in Fig.3, and were analyzed by the following coupled nonlinear rate equations[19,21]:

$$\begin{aligned}
\frac{dn_{\pm}}{dt} &= -\gamma_e n_{\pm} N_{\mp} - \frac{n_{\pm} - n_{\mp}}{2\tau_s} + G_{\pm} - \frac{n_{\pm}}{\tau_d} \\
\frac{dN_{\pm}}{dt} &= -\gamma_e n_{\mp} N_{\pm} - \frac{N_{\pm} - N_{\mp}}{2\tau_{sc}} + \frac{1}{2}\gamma_h p N_{\uparrow\downarrow} \\
\frac{dp}{dt} &= -\gamma_h p N_{\uparrow\downarrow} + G_{+} + G_{-} - \frac{n_{+} + n_{-}}{\tau_d} \\
N_c &= N_{\uparrow\downarrow} + N_{+} + N_{-}
\end{aligned} \tag{1}$$

Here $G_{\pm}$ is the photo-generation rate of free carriers and $n_{\pm}$ ($N_{\pm}$) the density of conduction electrons (the density of the defects occupied by a single electron), where the "±" signs refer to the electron spin orientations $S_z = \pm 1/2$. $N_{\uparrow\downarrow}$ corresponds to the concentration of the defects having two spin-paired electrons, and N_c the total defect concentration. The density of free holes is denoted by p. τ_s (τ_{sc}) is the spin relaxation times of conduction (localized) electrons. τ_d denotes the free carrier decay time, including all radiative and spin-independent non-radiative recombination channels except that via the spin-filtering defects. $\gamma_e(\gamma_h)$ is the trapping coefficient of free electrons (free holes) by the defects. In the analysis we use τ_d=10 ns, τ_{sc} =1.5 ns and τ_s=150 ps.[19,21] Here we assume that τ_d is governed by the radiative time of the BB PL transition. The analysis is not sensitive to τ_d as long as it is much longer than the electron capture & recombination time via the spin-filtering defects, i.e. $\tau_d >> (\gamma_e N_{\pm})^{-1}$ and $\tau_d >> (\gamma_h N_{\uparrow\downarrow})^{-1}$. The analysis is insensitive to τ_{sc}, as long as it is >1.5 ns. This leaves only γ_e/γ_h and $\gamma_e N_c$ as fitting parameters. As the absolute values of γ_e and defect concentration N_c cannot be

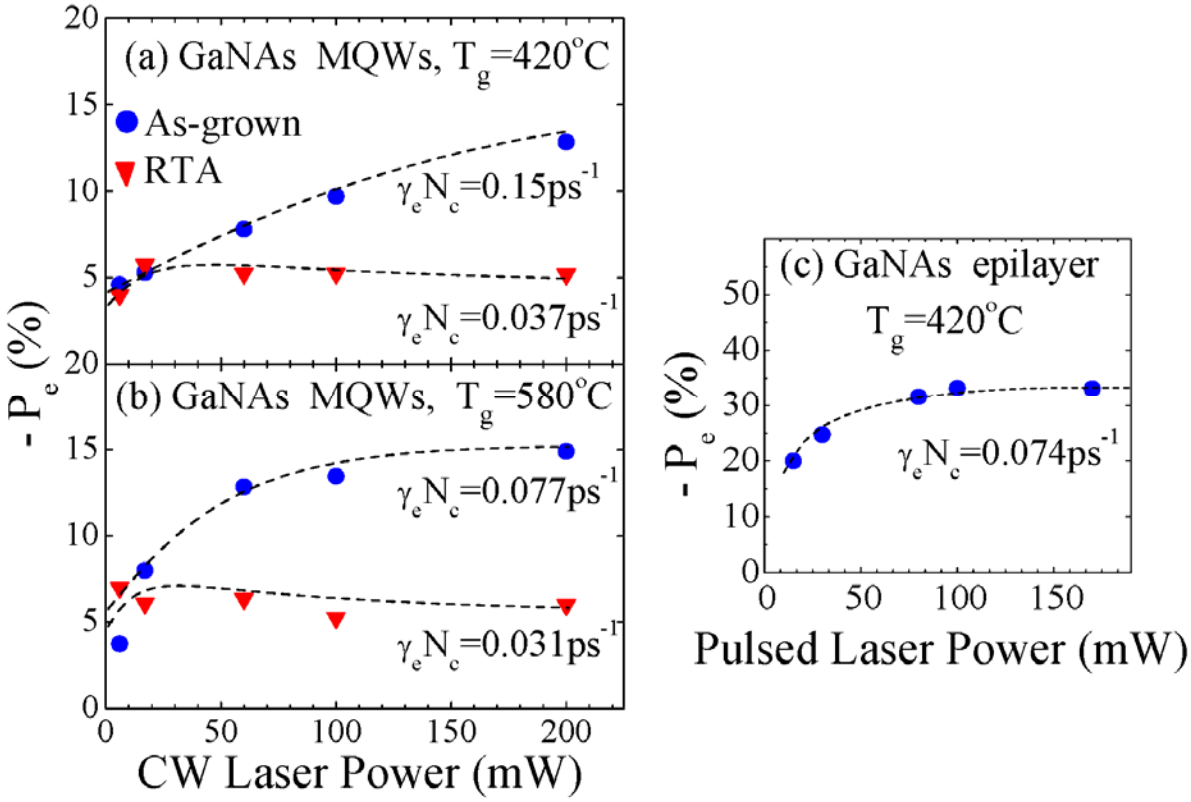

Figure 3: Dependence of conduction electron spin polarization on the optical excitation power and the concentration of the spin-filtering defects. *The dots denote the P_e values determined from the PL polarization of the e-hh transition detecting at the peak position of the PL spectra under σ^+ cw laser excitation at 840 nm, obtained from (a) the $GaN_{0.012}As_{0.988}$ MQWs grown at 420 °C and (b) the $GaN_{0.011}As_{0.989}$ MQWs grown at 580 °C. Results from both as-grown (filled circles) and RTA-treated (filled triangles) samples are shown. The time-integrated values of P_e from the $GaN_{0.0076}As_{0.9924}$ epilayer grown at 420 °C are shown in (c) by dots, obtained by detecting the PL polarization at 950 nm (see Fig.2a) under σ^+ pulsed laser excitation at 840 nm. The dashed lines are the simulated curves based on the best fit of Eq. 1 to the experimental results, yielding the fitting parameter $\gamma_e N_c$ for each sample. The results clearly show that P_e increases with increasing excitation intensity until the concentration of the photo-generated conduction electrons is comparable with that of the spin-filtering defects. With a further increase in the excitation density, P_e saturates, and even slightly decreases under the cw laser excitation, because the minority spins of the excess conduction electrons can no longer be depleted by the defects. The maximum value of P_e achievable in each sample is determined by its $\gamma_e N_c$ value and thus its defect concentration. Typically, higher P_e values were obtained under the pulsed laser excitation with a similar average laser power as compared with that under the cw laser excitation. This can be attributed to the much higher excitation density during the laser pulses and a discontinued supply of minority spins after the laser pulses, when the pulsed laser excitation was employed. All results were obtained at RT and B=0.*

determined independently here, we used a combined fitting parameter $\gamma_e N_c$ that is proportional to the capture rate of free electrons by the defects and can also be employed to compare relative defect concentrations in different samples. The fitting curves based on Eq.1 are displayed by the dashed lines in Fig.3, with γ_e/γ_h =4 and $\gamma_e N_c$ values given for each sample. The analysis reveals that the defect concentration increases with decreasing growth

temperature and increasing N concentration (not shown in Fig.3). Post-growth rapid thermal annealing (RTA) is found to significantly reduce the defect concentration by a factor of ~2-15. The observed increase of P_e with excitation power clearly manifests the spin-filtering effect.

To identify the exact chemical nature of the spin-filtering defects, we carried out a detailed study by optically detected magnetic resonance (ODMR). ODMR[23] is ideally suited here because it monitors both the conduction electron concentration (via the intensity of the BB PL) and the spin polarization of the electrons at the spin-filtering defects (via the ESR intensity that is proportional to $|N_+-N_-|$), as well as the link between them (via ODMR as a change in the intensity of the BB PL induced by the ESR transitions). Under σ^x excitation, an equal number of spin-up and spin-down conduction electrons are created. If the capture and annihilation of the electrons by the defects dominates over spin relaxation of both conduction and localized electrons, no population difference between the two spin states of the defects is expected, i.e., $|N_+-N_-|=0$, rendering a vanishing ESR (thus ODMR) signal. Under $\sigma^\pm$ excitation, on the other hand, the dynamic spin polarization of the electrons at the defects leads to a sizable $|N_+-N_-|$ and thus ESR. The ESR-induced spin flips of the spin-polarized defect electrons will open up an otherwise spin-forbidden recombination channel, see Fig.4a. This will lead to a reduction of free carrier concentrations and thus of the corresponding BB PL intensity, giving rise to a so-called ODMR signal. As examples, we show in Fig.4b typical ODMR spectra from GaNAs. As expected, a vanishingly weak ODMR signal was observed under σ^x excitation, whereas rather strong ODMR signals were observed under $\sigma^\pm$ excitation. These findings clearly show that a sizable spin polarization of the defect electrons was generated under $\sigma^\pm$ excitation, and a slight change of this polarization by the ESR directly affects the free carrier concentration proving the role of the defects in spin filtering.

A Ga_i self-interstitial is unambiguously identified by ODMR as the core of the spin-

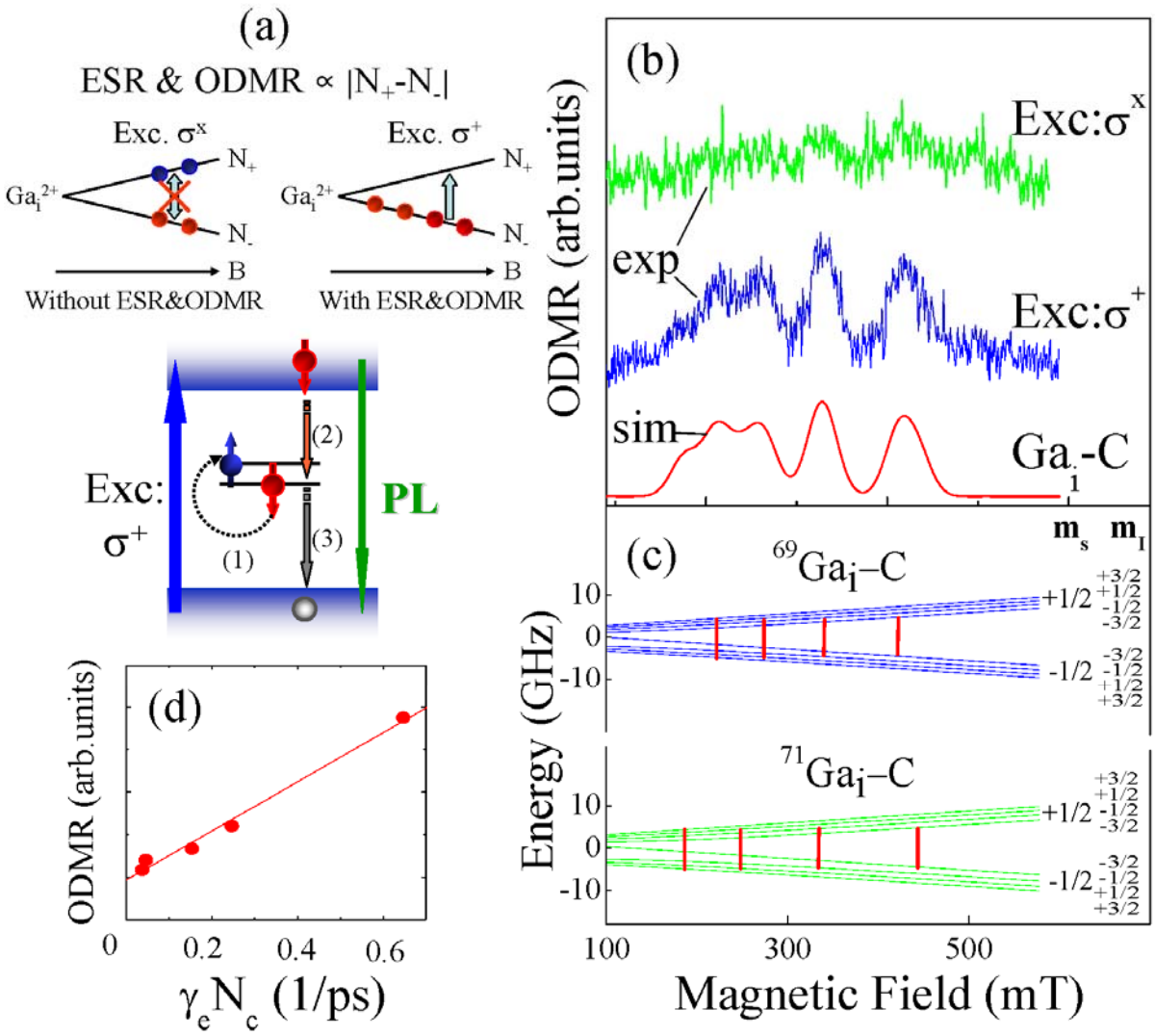

Figure 4: Identification of the spin-filtering defects by ODMR. *(a) Schematic pictures of the expected ESR transitions under σ^x and σ^+ excitation. In the former case, an equal population of the two electron spin states of the Ga_i^{2+} defects results in vanishing ESR and ODMR signals as the ESR and ODMR intensity is proportional to the population difference $|N_+-N_-|$. Under σ^+ excitation, on the contrary, a sizable $|N_+-N_-|$ induced by dynamical electron spin polarization leads to a detectable ESR transition between the two spin states. The ESR transition opens the otherwise spin-forbidden carrier capture and recombination channel, leading to a reduced number of free carriers available for the BB PL transition - an ODMR signal. The numbers in the parentheses indicate the sequence of events. (b) Typical ODMR spectra by monitoring the total intensity of the BB PL from an RTA-treated $GaN_{0.021}As_{0.979}$ epilayer, obtained at 3K under σ^x and σ^+ excitation at 850 nm. The microwave frequency used is 9.2823 GHz. A simulated ODMR spectrum of the identified Ga_i defect (denoted by Ga_i-C) is also shown. (c) Calculated energy levels associated with the electronic and nuclear spin states of the Ga_i^{2+} defect. The allowed ESR transitions ($\Delta m_S=\pm 1$ and $\Delta m_I=0$) occur when the electron spin splitting matches the microwave photon energy, and are marked by the vertical lines. The calculations and simulation were done with the aid of Eq. 2 by using the spin Hamiltonian parameters given in the text. (d) ODMR intensities from the identified Ga_i defects as a function of $\gamma_e N_c$. The latter are determined from the rate equation analyses (Eq.1). The line is a guide to the eye.*

filtering defects. This conclusion is based on the following experimental facts. Firstly, the observed multiple ODMR lines arise from a hyperfine structure derived from a strong interaction between an unpaired localized electron spin (S=1/2) and the nuclear spin of an atom that has two isotopes with a nuclear spin I=3/2 and a 60/40 ratio of natural abundance. This gives rise to four magnetic-dipole allowed ODMR transitions ($\Delta m_S=\pm 1$ and $\Delta m_I=0$) for each Ga isotope with an intensity ratio of 60/40, see Fig.4c. Ga is the only atom with such unique properties, i.e., two naturally abundant isotopes, ^{69}Ga (60.4% abundant) and ^{71}Ga (39.6% abundant), and I=3/2 for both isotopes. Secondly, the ODMR spectra are isotropic with a rotation of magnetic field **B** with respect to the crystallographic axes. This finding reveals that the electron wave-function at the defects should be s-like. This is consistent with the observed strong hyperfine interaction, as the s-like electron wavefunction results in a strong Fermi contact term. The involved defects should then be in the Ga_i^{2+} charge state occupied by a single unpaired electron with an electronic state of A_1 symmetry, as the alternative Ga_{As} antisite was predicted to possess a T_2-symmetry state[24,25]. To quantitatively confirm this identification, we have carried out a detailed analysis of the ODMR results by a spin Hamiltonian

$$H = \mu_B g \mathbf{B} \cdot \mathbf{S} + A \mathbf{S} \cdot \mathbf{I} . \qquad (2)$$

Here, μ_B is the Bohr magneton, g the electronic g-factor, and A the hyperfine parameter. g=2.000 (2.005), A(^{69}Ga)=620 (770) x10^{-4} cm^{-1} and A(^{71}Ga)=788 (1000)x10^{-4} cm^{-1} are obtained from a best fit to the experimental data for the Ga_i defects in the RTA-treated (as-grown) samples. The ratio A(^{71}Ga)/A(^{69}Ga) is in excellent agreement with that of their nuclear magnetic moments μ(^{71}Ga)/μ(^{69}Ga)=1.27. A simulated ODMR spectrum by Eq.2 using the obtained parameters is displayed as Ga_i-C in Fig.4b, showing excellent agreement with the experimental data. The difference between the Ga_i defects in the RTA and as-grown samples lies at their neighbouring atoms and geometric locations. By using a one-electron

linear combination of atomic orbital scheme[26] and the charge density of the 4*s* electron $|\psi_{4s}(0)|^2$ =72.7x10^{24} cm^{-3} for a free neutral Ga atom[25,27], the localization of the electron wave functions at the Ga_i^{2+} defects is estimated to be 20% (as-grown) and 16% (RTA). The rather strong localization shows that they are deep-level defects, a prerequisite for efficient carrier recombination.

To further quantitatively confirm that the identified Ga_i defects are indeed responsible for the spin filtering, we examined their ODMR intensity as a function of the spin-filtering defect concentrations deduced by Eq.1. The excellent correlation, shown in Fig.4d, provides further support for the predominant role of these Ga_i defects in spin filtering that has led to the observed strong P_e at RT.

Further improvements in the efficiency of the defect-engineered spin-filtering can be envisioned by (i) increasing the ratio between the capture rate of conduction electrons by the Ga_i defects ($\propto \gamma_e N$) and the spin relaxation rate of conduction electrons ($1/\tau_s$), and (ii) increasing the ratio between $\gamma_e N$ and the spin-independent carrier recombination rate ($1/\tau_d$) via other defects. Indeed the spin relaxation of conduction electrons tends to drive P_e towards zero value at thermal equilibrium (B=0). Spin-independent carrier recombination via other defects equally depletes conduction electrons of both spins, competing with spin-filtering. The maximum P_e value is expected to approach 100% when $\gamma_e N >> 1/\tau_s$ and $1/\tau_d$, independent of initial spin polarization of the incoming electrons before being spin filtered. Future efforts should therefore focus on prolonging the spin relaxation time of conduction electrons[28] and increasing the concentration of the spin-filtering defects without introducing other competing, spin-independent carrier recombination centers.

So far there is a lack of an efficient room temperature spin filter – a key element for spintronics, despite intense efforts. This work demonstrates a significant development of our ability in drastically increasing spin-filtering efficiency at RT by purposely introducing spin-

filtering defects. Our approach offers another attractive feature - the freedom and ease in switching the spin direction of the spin filters by reversing electron spins of spin-filtering defects either optically or electrically. The proposed spin filtering can not only generate P_e or amplify weak P_e, but also detect spin polarization of injected electrons by monitoring the ratio between the numbers of electrons passing and being blocked by the spin filter. This work has thus demonstrated the potential of defect-engineered, switchable spin filters for creating, amplifying and detecting electron spin polarization at RT in a non-magnetic semiconductor without requiring external magnetic fields, desirable for practical device applications.

Methods

Samples. The dilute nitride GaNAs samples were grown by gas-source as well as solid-source molecular beam epitaxy (MBE) on (100)-oriented semi-insulating GaAs substrates with a 2500Å-thick GaAs buffer. Two types of samples were studied: (i) 7-period GaAs/GaNAs (200/70Å) multiple-quantum-wells (MQWs) structures. They were grown either at T_g = 420 ^oC with N composition [N]=1.2% and 2% or at 580 ^oC with [N]=1.1%; and (ii) GaNAs epilayers (about 0.1 μm thickness) with [N]=0.76%-2.1%, grown at 420 ^oC. Post-growth RTA was carried out at 850 ^oC for 10 s with a halogen lamp in a flowing N_2 ambient.

Dynamical polarization of the spin-filtering Ga_i defects. In our experiments, the initial spin polarization of conduction electrons was generated by circularly polarized light excitation at energy above the e-hh and e-lh BB transition in GaNAs, taking advantage of the selection rules and the three-fold higher oscillator strength of the e-hh optical transition as compared to the e-lh transition[15]. A spin polarized conduction electron can only be captured by the Ga_i^{2+} defect if the first localized electron has a spin orientation opposite to that of the conduction electron, due to the Pauli exclusion principle. After the subsequent recombination between

one of two localized electrons and an unpolarized free hole (due to much faster spin relaxation), a half number of the Ga_i^{2+} are left with a localized electron with its spin orientation parallel to that of the conduction electrons. Such a continuous SDR process[16-21] will dynamically polarize the spin of the first localized electrons at the Ga_i^{2+} towards that of conduction electrons.

Experimental techniques. Both cw and time-resolved PL experiments were performed at RT and at zero magnetic field. Photo-excitation above the bandgap energy of GaNAs was provided by circularly polarized light (and linearly polarized light) from a Ti:sapphire laser at a wavelength of 840-855 nm, propagating along the direction normal to the sample surface. Laser power of up to 200 mW was used with a typical spot size of about 0.1 mm. The resulting polarized PL was measured in a back-scattering geometry. In time-resolved PL experiments, the samples were excited by 1.5 ps pulses generated by a mode-locked Ti:sapphire laser with a repetition frequency of 80 MHz. The time resolved PL was then recorded using a streak camera with an overall time-resolution of 8 ps.

The ODMR experiments were done at 2.5-300 K with a modified ESR spectrometer working at the X-band (~9.3 GHz). PL was excited by a Ti:sapphire laser at a wavelength of 850 nm. The ODMR signals were detected as spin resonance induced changes of the PL intensity monitored by a cooled Ge detector with a proper selection of optical filters.

References

1. Wolf S.A. et al, Spintronics: A spin-based electronics vision for the future. *Science* **294**, 1488-1495 (2001).

2. Žutić I., Fabian J. & Das Sarma S., Spintronics: Fundamentals and applications. *Rev. Mod. Phys.* **76**, 323-410 (2004).

3. Awschalom D.D. & Flatté M.E., Challenges for semiconductor spintronics. *Nature Phys.* **3**, 153-159 (2007).

4. Chappert C., Fert, A. & Nguyen Van Dau F., The emergence of spin electronics in data storage. *Nature Mater.* **6**, 813-823 (2007).

5. Zhu H.J. et al, Room-temperature spin injection from Fe into GaAs. *Phys. Rev. Lett.* **87**, 016601 (2001).

6. Hammar P. R. & Johnson M., Detection of spin-polarized electrons injected into a two-dimensional electron gas. *Phys. Rev. Lett.* **88**, 066806 (2002).

7. Jiang X. et al, Highly Spin-Polarized Room-Temperature Tunnel Injector for Semiconductor Spintronics using MgO(100). *Phys. Rev. Lett.* **94**, 056601 (2005).

8. Jonker B.T. et al, Electrical spin-injection into silicon from a ferromagnetic metal/tunnel barrier contact. *Nature Phys.* **3**, 542-546 (2007).

9. Fiederling R. et al, Injection and detection of a spin-polarized current in a light-emitting diode. *Nature* **402**, 787-790 (1999).

10. Ohno Y. et al, Electrical spin injection in a ferromagnetic semiconductor heterostructure. *Nature* **402**, 790-792 (1999).

11. Potok R.M. el al, Detecting Spin-Polarized Currents in Ballistic Nanostructures. *Phys. Rev. Lett.* **89**, 266602 (2002).

12. Folk J.A. et al, A gate-controlled bidirectional spin filter using quantum coherence. *Science* **299**, 679-682 (2003).

13. Hauptmann J.R. et al, Electric-field-controlled spin reversal in a quantum dot with ferromagnetic contacts. *Nature Phys.* **4**, 373-376 (2008).

14. Gajek M. et al, Tunnel junctions with multiferroic barriers. *Nature Mater.* **6**, 296-302 (2007).

15. Meier, F. & Zakharchenya, B.P., *Optical Orientation*. (North-Holland, Amsterdam, 1984).

16. Weisbuch C. & Lampel G., spin-dependent recombination and optical spin orientation in semiconductors. *Solid. State. Comm*. **14**, 141 (1974).

17. Miller R. C., Tsang W. T. & Nordland W. A., Spin-dependent recombination in GaAs. *Phys. Rev*. B **21**, 1569-1575 (1980).

18. D. Paget, Optical-pumping study of spin-dependent recombination in GaAs. *Phys. Rev. B*. **30**, 931-946 (1984).

19. Kalevich, V.K. et al, Spin-dependent recombination in GaAsN solid solutions. *JETP Lett*. **82**, 455–458 (2005).

20. Lombez L. et al, Spin dynamics in dilute nitride semiconductors at room temperature. *Appl. Phys. Lett.* **87**, 252115 (2005).

21. Lagarde D. et al, Electron spin dynamics in GaAsN and InGaAsN structures. *Phys. Stat. Sol. (a)* **204**, 208–220 (2007).

22. For a review on GaNAs, see e.g. Buyanova I.A. & Chen W.M., *Physics and Applications of Dilute Nitrides*. (Taylor & Francis Books, Inc., New York, 2004).

23. For a review on ODMR, see e.g. Chen W.M., Applications of optically detected magnetic resonance in semiconductor layered structures. *Thin Solid Fi*lms **364**, 45-52 (2000).

24. Baraff G. A. & Schluter M., Electronic Structure, Total Energies, and Abundances of the Elementary Point Defects in GaAs. *Phys. Rev. Lett*. **55**, 1327-1330 (1985).

25. Thinh N. Q. et al, Properties of Ga-interstitial defects in AlGaNP. *Phys. Rev. B* **71**, 125209/1-9 (2005).

26. Watkins G. D. & Corbett J. W., Defects in Irradiated Silicon. I. Electron Spin Resonance of the Si-A Center. *Phys. Rev.* **121**, 1001-1014 (1961).

27. Koh A. K. & Miller D. J., *Atomic Data and Nuclear Data Tables* **33** 235-253 (1985).

28. Ohno Y. et al, Spin Relaxation in GaAs(110) Quantum Wells. *Phys. Rev. Lett.* **83**, 4196-4199 (1999); D'yakonov M.I. & Kachorovskii V. Yu, Spin relaxation of two-dimensional electrons in noncentrosymmetric semiconductors. *Sov. Phys.Semicond.* **20**, 110-112 (1986).

Acknowledgements

W.M. Chen and I.A. Buyanova gratefully acknowledge the support from Linköping University through the Professor Contracts, the Swedish Research council (VR), the Swedish Energy Agency, the Knut and Alice Wallenberg Foundation, the Wenner-Gren Foundations, and the Swedish Foundation for International Cooperation in Research and Higher Education (STINT). The work at UCSD is partially supported by NSF Grant No. DMR-0606389.

Author information

Reprints and permissions information is available online at http://npg.nature.com/reprintsandpermissions. Correspondence and requests for materials should be addressed to W.M.C or I.A.B.